HHS Public Access

Author manuscript

Biomaterials. Author manuscript; available in PMC 2023 May 01.

Published in final edited form as:

Biomaterials. 2022 May ; 284: 121490. doi:10.1016/j.biomaterials.2022.121490.

A clinically relevant formulation for direct administration of nerve specific fluorophores to mitigate iatrogenic nerve injury

Connor W. Barth[1,§], **Vidhi M. Shah**[3,§], **Lei G. Wang**[1], **Anas M. Masillati**[1], **Adel Al-Fatease**[3], **Syed Zaki Husain Rizvi**[3], **Alexander L. Antaris**[4], **Jonathan Sorger**[4], **Deepa A. Rao**[5], **Adam W.G. Alani**[1,2,3], **Summer L. Gibbs**[1,2,*]

[1]Biomedical Engineering Department, Oregon Health & Science University, Portland, OR 97201

[2]Knight Cancer Institute, Oregon Health & Science University, Portland, OR 97201

[3]Department of Pharmaceutical Sciences, College of Pharmacy, Oregon State University, Portland, OR, 97201

[4]Intuitive Surgical, 1020 Kifer Road, Sunnyvale, CA 94086

[5]School of Pharmacy, Pacific University, Hillsboro, OR 97123

Abstract

[*]Corresponding Author: Summer L. Gibbs, Ph.D., Oregon Health & Science University, 2730 S Moody Ave, Mail Code: CL3SG, Portland, OR 97201, gibbss@ohsu.edu, Phone: 503-494-8940; **MATERIALS & CORRESPONDANCE**: All correspondence and request for materials can be sent to Dr. Summer Gibbs at gibbss@ohsu.edu.

[§]Authors contributed equally to this work

AUTHOR CONTRIBUTIONS

C.W.B., V.M.S., L.G.W., A.W.G.A. and S.L.G. designed all experiments. L.G.W. synthesized LGW01-08, the oxazine derivative tested herein. V.M.S., A.A.F., S.Z.H.R. and A.W.G.A. designed, developed and validated the formulation strategies. C.W.B., A.M.M. and V.M.S. performed all murine experimental studies. C.W.B., L.G.W., A.L.A. and J.S. performed the swine studies. D.A.R. assisted with the LCMS/MS analysis of the blood and tissue lysates. C.W.B. and V.M.S. analyzed all collected data. C.W.B., V.M.S., A.W.G.A. and S.L.G. wrote and edited the manuscript. S.L.G. supervised the project.

COMPETING INTERESTS

Alexander Antaris and Jonathan Sorger are employees of Intuitive Surgical. Lei Wang, Connor Barth and Summer Gibbs are inventors on patent application PCT/US19/43739 held by Oregon Health and Science University that cover the composition and methods of use of the nerve-specific oxazine compounds discussed in this manuscript. Summer Gibbs, Connor Barth, Adam Alani, Vidhi Shah, and Lei Wang are inventors on patent application PCT/US19/045347 held by Oregon Health and Science University and Oregon State University that cover the composition and methods of use of the formulations discussed in this manuscript. Lei Wang, Connor Barth and Summer Gibbs and also co-founders of Inherent Targeting, LLC.

Declaration of interests

The authors declare the following financial interests/personal relationships which may be considered as potential competing interests: Summer Gibbs reports a relationship with Inherent Targeting, LLC that includes: equity or stocks. Connor Barth reports a relationship with Inherent Targeting, LLC that includes: equity or stocks. Lei Wang reports a relationship with Inherent Targeting, LLC that includes: equity or stocks. Jonathan Sorger reports a relationship with Intuitive Surgical Inc that includes: employment. Alexander Antaris reports a relationship with Intuitive Surgical Inc that includes: employment. Summer Gibbs has patent #PCT/US19/43739 pending to Oregon Health & Science University. Connor Barth has patent #PCT/US19/43739 pending to Oregon Health & Science University. Lei Wang has patent #PCT/US19/43739 pending to Oregon Health & Science University. Summer Gibbs has patent #PCT/US19/045347 pending to Oregon Health & Science University, Oregon State University. Connor Barth has patent #PCT/US19/045347 pending to Oregon Health & Science University, Oregon State University. Lei Wang has patent #PCT/US19/045347 pending to Oregon Health & Science University, Oregon State University. Adam Alani has patent #PCT/US19/045347 pending to Oregon Health & Science University, Oregon State University. Vidhi Shah has patent #PCT/US19/045347 pending to Oregon Health & Science University, Oregon State University.

Iatrogenic nerve injury significantly affects surgical outcomes. Although intraoperative neuromonitoring is utilized, nerve identification remains challenging and the success of nerve sparing is strongly correlated with surgeon experience levels. Fluorescence guided surgery (FGS) offers a potential solution for improved nerve sparing by providing direct visualization of nerve tissue intraoperatively. However, novel probes for FGS face a long regulatory pathway to achieve clinical translation. Herein, we report on the development of a clinically-viable, gel-based formulation that enables direct administration of nerve-specific probes for nerve sparing FGS applications, facilitating clinical translation via the exploratory investigational new drug (eIND) guidance. The developed formulation possesses unique gelling characteristics, allowing it to be easily spread as a liquid followed by rapid gelling for subsequent tissue hold. Optimization of the direct administration protocol with our gel-based formulation enabled a total staining time of 1-2 minutes for compatibility with surgical procedures and successful clinical translation.

INTRODUCTION

Iatrogenic nerve damage represents a major surgical comorbidity, significantly affecting postsurgical quality of life.[1] Despite the surgical practice of nerve sparing techniques for decades, intraoperative nerve identification and sparing remain difficult and success rates are strongly correlated with surgeon experience level and ability to master techniques.[2–4] Intraoperative nerve damage affects all surgical specialties and represents a significant challenge even for high volume surgeries such as prostatectomy, hysterectomy, hernia repair, and thyroidectomy.[5–8] Around 12% of the United State population will develop a thyroid condition in their lifetime, where surgery is a common treatment.[9] Notably, thyroidectomy is a surgical procedure particularly plagued by nerve damage, where voice changes caused by injury to the recurrent laryngeal nerves (RLN) affects up to 15% of patients and comprises 46% of all malpractice-related claims for endocrine surgery.[10–12] In rare occurrences, bilateral injury to the RLN can cause adduction of the vocal cords, a life threatening complication resulting in airway collapse.[10] Rates of postoperative complications are associated with surgeon experience level, where low volume centers show a substantial decrease in positive outcomes.[13] At present, the majority of thyroidectomies are implemented outside of high volume centers, with 50% of procedures completed by surgeons who perform fewer than five cases annually.[14] Intraoperative detection and monitoring of the vital RLN structure is currently performed via white light visualization or electromyography.[15] However, the RLN is a small caliber nerve that runs directly beneath the thyroid with a widely varied course relative to the thyroid anatomy.[16] Intraoperative neuromonitoring (INM) methods are employed to assist surgeons in sparing the RLN and are utilized in >80% of procedures worldwide.[17] Yet, INM requires a lengthy learning curve and can only provide intermittent nerve function and location assessment, demonstrating little to no improvement over dissection and direct visualization of the RLN.[15] In response to these challenges, other technologies have been developed to enhance the identification of nerve tissue in the head and neck region including ultrasound, optical coherence tomography, and polarimetric imaging strategies.[18–21] However, these lack wide-field imaging capabilities and/or demonstrate low sensitivity and specificity for smaller, buried nerves such as the RLN. While direct visualization of the RLN remains the clinical gold standard for nerve sparing, it is often buried beneath the thyroid, as well as the surrounding

muscle and adipose tissues, making consistent nerve identification and visualization a significant challenge.[16]

Fluorescence-guided surgery (FGS) shows promise for enhanced visualization of specifically highlighted tissues intraoperatively. FGS offers high sensitivity, wide-field, real-time imaging, and with optimized molecular specific probes, targeted tissues could be identified at up to centimeter depths.[22] Several FGS systems have already demonstrated benefits for thyroidectomy procedures, where near-infrared (NIR) autofluorescence imaging facilitates improved identification and preservation of the parathyroid gland, preventing hypoparathyroidism and subsequent hypocalcemia.[23–33] Utilizing FGS for nerve identification and sparing during thyroidectomy could provide similar patient outcome benefits, however a nerve-specific fluorophore is required for successful visualization, where a NIR agent would have the added benefit of enabling buried nerve identification. Several classes of small molecule fluorophores have demonstrated nerve specificity in preclinical models.[24, 34–44] Of these, oxazine 4 has shown promise for further translation with a red-shifted absorption and emission and high nerve specificity in murine and porcine nerve models.[44] Recently, our group has successfully synthesized NIR analogs oxazine 4, resulting in improved nerve detection at depth.[45, 46] However, clinical translation of novel contrast agents requires an extensive regulatory pathway where a successful investigational new drug (IND) application is necessary for safe first-in-human use.

Direct contrast agent administration is an attractive alternative to systemic administration of fluorescent probes to minimizing the required dose to generate tissue-specific contrast, resulting in eased regulatory burdens for first-in-human studies.[47] By selectively labeling tissues only within the surgical field, direct administration requires a significantly lower dose than systemic administration to generate clinically useful contrast. Recently, we developed a direct administration methodology that provides equivalent nerve signal to background (SBR) to systemic administration following a 15-minute staining protocol.[48] This direct administration methodology resulted in >15x lower optimal dose vs. systemic administration and when body surface area scaled to humans, the optimal direct administration dose falls within the requirements for clinical translation under an exploratory IND (eIND). Notably, studies conducted under an eIND require limited preclinical toxicity testing, since only a microdose (<100 μg) is administered to each patient, significantly reducing the timeline and overall cost of first-in-human studies.

While the previously developed direct administration methodology provided high nerve specificity and SBR in rodent models using a short staining protocol,[48] preliminary studies in large preclinical models (i.e., swine) resulted in substantial background staining, decreasing nerve contrast. Additionally, the direct administration methodology utilized a co-solvent formulation containing dimethyl sulfoxide (DMSO) and Cremophor to solubilize the fluorophore, which limit clinical translation due to potential vehicle induced toxicity challenges.[49] To faciliate future clinical translation, hydogels used in previously food and drug administration (FDA) approved formulation strategies were investigated herein. Hydrogels are a three-dimensional network of polymers, which can absorb and retain substantial amounts of water, facilitating a critical solution transition from a fully miscible solution to a gel. This sol to gel (i.e., gelation) transition is induced by either chemical

stimuli (e.g., polymer concentration, complexation) or physical stimuli (e.g., temperature, light).

Hydrogels have been successfully utilized in non-invasive imaging technologies such as magnetic resonance imaging and computed tomography to functionally encapsulate and deliver contrast agents, enabling monitoring of surgical or therapeutic treatments or implanted medical devices.[50–53] Herein, Alginate and Pluronics® (BASF) or Poloxamers (ICI) were investigated as possible methods to facilitate increased application control on a variety of tissue surfaces, angles, and morphologies using our previously validated NIR nerve-specific probe, LGW01-08.[45] Alginate hydrogels are naturally-sourced, biocompatible, anionic polysaccharide that undergo irreversible gelation via ionic or covalent cross-linking process and are used in a variety of biomedical applications.[54] Sodium (Na) Alginate has been reported to provide excellent coverage of the applied surface and enhanced permeability via a thin hydrogel film that forms after the compound's interaction with divalent metal ions, such as the calcium (Ca^{+2}), present in live tissues.[54, 55] Pluronics or Poloxamers are polymers synthesized by condensation of ethylene oxide and propylene oxide,[56] where the number of the repeating unit can be varied for polymers with different physiochemical properties. Pluronics are widely used as non-ionic surfactants, solubilizers, and drug delivery systems and are used as excipients in FDA approved products.[57] Pluronics F127 is a thermo-reversible temperature-responsive polymer that exhibits a lower critical solution temperature and undergoes sol-to-gel transition with warming,[58] making it an attractive formulation excipient for its potential to maintain a solidified state when applied in the surgical field. Additionally, Pluronics F127, is a surfactant and has been shown to increase both the apparent aqueous solubility of hydrophobic molecules and their tissue penetration.[59–61] Furthermore, Pluronics F127 and Na Alginate hydrogels have been reported to provide a basis for foam formulations such as those used clinically during surgery.[62–64] Modeled after the gel and foam based formulations used clinically as intraoperative hemostatic agents and surgical sealants (e.g., FloSeal, Surgiflo, and Duraseal), we have developed a hydrogel based formulation using clinically approved F127 Pluronics, which has attractive gelling characteristics for FGS applications. Herein, F127 Pluronics was used to solubilize LGW01-08 to develop a clinically relevant direct administration methodology, resulting in a 1-2 minute staining protocol that provided nerve SBR >2. Our optimized direct administration methodology will enable rapid and successful clinical translation of nerve-targeted FGS for improved nerve identification, visualization and sparing during surgery.

RESULTS

Formulation composition, stability, and release.

The hydrogel formulations tested herein were chosen for their stability, clinical approval status, viscosity, gelation profile, and tissue penetration characteristics. The range of concentrations of each of these selected hydrogels was chosen to provide acceptable syringeability of the solution before gelation and to ensure the transition from liquid to gel when exposed to tissue in the surgical environment.

Na Alginate viscosity measurements at three concentrations (5.0%, 6.5% and 8.0%) in the absence of a divalent ions exhibited a Newtonian system, where the viscosity did not change as a function of shear rate (Fig. S1A). When 6.5% Na Alginate solution was exposed to Ca^{+2} ions at varied concentrations (2 nM, 2 μM and 2 mM) in solution, the gel showed increase in shear rate for the 2 nM and 2 μM Ca^{+2}, while the 2 μM and 2 mM Ca^{+2} gels showed the same shear rate, demonstrating that the viscosity of the 6.5% Na Alginate was dependent on the calcium concentration and the 2 μM Ca^{+2} ions was at or above viscosity saturation (Fig. S1B). Three concentrations of Pluronics F127 were prepared at 20%, 22% and 25%. The 22% and 25% solutions exhibited a non-Newtonian shear thinning system, while the 20% solution exhibited Newtonian flow behavior (i.e., no change in viscosity, Fig. S1C). The viscosity of these solutions showed a biexponential relationship with temperature, where temperatures below 33 °C showed no change in viscosity. Temperature greater than 33 °C showed a concentration dependent, exponential increase in viscosity (Fig. S1D). Thus, the sol-to-gel transition temperature was determined to be 33 °C for the 22% and 25% polymer solutions (Fig. S1D).

LGW01-08 was fully released from Na Alginate and Pluronic F127 after 192 h (8 days) and 276 h (11.5 days), respectively under sink conditions (Fig. S2). Visual inspection showed that both gels remained intact throughout the study. The coefficient of determination (R^2) for Na Alginate and Pluronics F127 gel were 0.977 and 0.997, respectively. The releases profiles show two phases: a fast and a slow release. Approximately 3% of LGW01-08 was released from the Pluronics F127 during the fast-release phase with a half-life of 4.04 h, followed by the slow-release phase in which 97% of the drug was released with a half-life of 217.9 h. In comparison, approximately 7% of the LGW01-08 was released from the Na Alginate during the fast-release phase with a half-life of 0.99 h tailed by the slow-release phase where 93% of the dye was released with a half-life of 76.87 h.

Murine nerve specificity screening using hydrogel-based formulations.

Na Alginate and Pluronics were used to create gel formulations for administration of the nerve specific fluorophore LGW01-08. Mouse brachial plexus and sciatic nerves were stained using direct administration with the varying concentrations of each hydrogel (n=6 per group; 5, 6.5, and 8% Na Alginate; 20, 22, and 25% Pluronics) to solubilize 50 μg/mL LGW01-08. The staining results were compared to the previously utilized liquid-based co-solvent formulation containing an equivalent LGW01-08 concentration (Fig. 1). No appreciable differences in nerve-specific highlighting were observed for the tested concentrations of Na Alginate or Pluronics compared to the previously utilized co-solvent formulation (Fig. 1A). No significant difference in nerve SBRs were observed using any specific formulation and all LGW01-08 stained groups had significantly higher nerve to muscle (N/M, p = <0.0001; 0.0002, 0.0037, 0.0009; <0.0001, 0.0013, and 0.0006 for control vs. co-solvent; 5, 6.5, and 8% Na Alginate; 20, 22, 25% Pluronics, respectively, Fig. 1C), nerve to adipose (N/A, p = <0.0015; <0.0001, 0.0025, <0.0001; <0.0002, 0.0005, and <0.0001 for control vs. co-solvent; 5, 6.5, and 8% Na Alginate; 20, 22, 25% Pluronics, respectively, Fig. 1D), and nerve to cut muscle (N/CM, p = <0.0001; 0.0002, 0.0037, 0.0009; <0.0001, 0.0013, and 0.0006 for control vs. co-solvent; 5, 6.5, and 8% Na Alginate; 20, 22, 25% Pluronics, respectively, Fig. 1E) ratios compared to the control unstained group.

Additionally, aside from the highest tested concentrations of Pluronics (i.e., 25% Pluronics, $p = 0.0057$) all hydrogel-based formulations displayed similar nerve tissue fluorescence intensities to the co-solvent formulation (Fig. 1B).

Hydrogel formulation viscosity assessment in large animal models.

Tissue spread in swine after hydrogel application was used as a metric to assess the future clinical utility of the viscosity enhancement for each formulation. Tissue spread was calculated using hydrogel-based formulations with 5.0, 6.5, and 8.0% Na Alginate as well as 20, 22, and 25% Pluronics at varying degrees of tilt (0°, 35°, and 65°, Fig. 2A). The lowest concentration of each viscosity enhancer tested (5.0% Na Alginate and 20% Pluronics) provided little resistance to spread at increased tilt angles and saw significant increases in the measured spread surface area at 35° and 65° tilts. The middle concentration of each viscosity enhancer tested (6.5% Na Alginate and 22% Pluronics) provided adequate tissue surface hold and did not see a large increase in surface area spread at higher degrees of tilt. The highest concentration of each viscosity enhancer tested (8.0% Na Alginate and 25% Pluronics) allowed only minimal initial tissue spread and no changes in tissue spread at higher tilt angles (Fig. 2B). The tradeoff between ability to spread following initial application and subsequent hold at more vertical surface angles were considered for clinical utility, permitting selection of the middle concentrations (6.5% Na Alginate and 22% Pluronics) as the most clinically relevant for each hydrogel formulation. Additionally, Pluronics was found to have more favorable gelling characteristics compared to Na Alginate in the large animal model. Specifically, since the viscosity of Pluronics increases at body temperature and decreases at cooler temperatures, including room temperature its properties facilitate ready application to a tissue surface. By comparison, Na Alginate increased viscosity at cooler temperatures and decreases viscosity at higher temperatures, making both application and tissue gelling less advantageous in these clinically relevant model systems.

Swine iliac plexus nerves were stained via direct administration of oxazine 4 formulated in 22% Pluronics, 6.5% Na Alginate and co-solvent formulation to further evaluate the performance of each hydrogel-based formulation in a clinically relevant surgical model (Fig. 2C). Staining with liquid co-solvent formulation required tenting of the surrounding tissue to collect runoff from the near vertical surface of the iliac plexus, generating significant pooling and difficulty controlling the stained area (Movie S1). This resulted in substantial background signal in the areas where the fluorophore pooled and an overall decrease in nerve to background tissue ratios (Fig. 2C). Staining with the Pluronics formulation resulted in facile application to the surgical site using a syringe and surgical tubing passed through the assist port of the da Vinci system as a liquid, where the hydrogel-based formulation immediately gelled upon contact with the iliac plexus nerve site, providing the desired tissue hold for the entire 5-minute incubation period (Movie S2). The resulting fluorescence images showed clear identification of the iliac nerve as well as adjacent buried nerve tissue and decreased background tissue staining vs. the liquid co-solvent formulation (Fig. 2C). The Na Alginate formulation provided an initially controlled application as a gel, but began to liquify and run from the nerve site into the body cavity as it warmed (Movie S3). Thus, increased background was observed in the resulting fluorescence images as compared to the Pluronics formulated fluorophore (Fig. 2C). Due to these additional advantages, Pluronics

was chosen as the optimal hydrogel since it allowed for initial tissue spreading with relative ease and subsequently gelled quickly, remaining at the site of application in the body cavity and resulted in specific nerve staining while minimizing background tissue uptake.

Direct administration methodology optimization.

The direct administration protocol with 22% Pluronics was optimized with the overall goal of a short staining protocol to highlight nerve tissue for future clinical translation. LGW01-08 concentration and incubation time were evaluated to minimize dose and staining time, where the highest tested concentration (i.e., 200 μg/mL) was the largest dose that would still fall within the microdosing range permitting first in human studies under an eIND. Nerve contrast and SBRs were similar between tested concentrations (25, 50, 200 μg/mL) and incubation times (1 and 5 mins, n = 6 nerve sites per staining condition, Fig. 3A). However, fluorescence signal intensities decreased at lower concentrations and incubation times (Fig. 3B) even though nerve SBRs were similar (Fig. 3C–3E). The highest tested concentration (i.e., 200 μg/mL) was selected for future studies as it maintained high nerve tissue fluorescence intensity at the short 1-minute total staining time, resulting in high nerve contrast.

The washing protocol parameters were investigated to determine the minimal amount of washing required to generate useful nerve tissue contrast. Room temperature (RT, 20-22 °C) and cold (~4 °C) phosphate buffered saline (PBS) were tested as the washing solutions with the hypothesis that cold PBS could more readily solubilize the Pluronics hydrogel. Short flushes were used to wash the nerve sites following staining with 200 μg/mL LGW01-08 in 22% Pluronics for 1 min (Fig. 4). Increased nerve contrast was observed after one to two washes, where additional washes further decreased background muscle and adipose fluorescence intensities (Fig. 4A). Quantified nerve tissue intensities and SBRs agreed with this observation for both the cold and RT PBS washes (Fig. 4B). After six washes, nerve intensities and SBRs were relatively constant, with minimal change between the 6^{th} and 18^{th} wash steps, demonstrating that six total washes generated nerve-specific contrast. Cold and RT PBS washes did not change nerve contrast appreciably and thus temperature was not deemed an important factor in overall wash performance. Following washing completion, images were collected every five min for up to 30 min to determine the effect of clearance on nerve signal intensities and SBRs (Fig. 4C). No significant change in nerve signal and slight yet not significant increases in the nerve SBRs occurred during this period, demonstrating robust nerve contrast generated from direct Pluronics formulated administration of LGW01-08.

Tissue staining penetration and diffusion quantification.

Stain penetration depth was assessed on murine muscle tissue stained with the optimized direct administration procedure. The stained muscle tissue was resected, flash frozen and cross-sectioned, facilitating quantification of diffusion profiles (n = 3 sections, Fig. 5). The average fluorescence intensity line profile demonstrated ~600 μm depth penetration following 1 min of Pluronics formulated LGW01-08 before fluorescence intensities returned to tissue autofluorescence levels (Fig. 5A & 5B). Fitting a mathematical model to the average diffusion curve allowed quantification of the diffusion coefficient and calculated

tissue penetration depths at varied incubation times (Fig. 5C). Using fluorescence reference standards 0.2 μg/mL was identified as the lowest concentration detectable when imaged beneath 1 mm of mouse muscle tissue. With this detection limit determined, calculated tissue penetration profiles showed that nerve buried beneath up to 500 μm of tissue could be stained and imaged following 1 min of incubation, where nerves buried beneath up to 1 mm of tissue could be stained and imaged following 5 min of incubation (Fig. 5D & 5E).

Rodent toxicology testing.

Toxicology testing was performed in rodents for the selected 22% Pluronics formulation with and without LGW01-08 loading. Subcutaneous injection was utilized as a surrogate for direct administration, with a 1.8 mg/kg dose used in the LGW01-08 administered group or ~7x the chosen dose from method optimization and 100x the maximum dose allowed for microdose studies when scaled by body surface area to humans. Pluronics loaded (i.e., with LGW01-08) and unloaded formulations were subcutaneously administered to assess any blood chemistry changes and effect on 14-day weight gain as compared to control animals (n = 5 mice per cohort, Fig. 6). Blood markers for kidney (blood urea nitrogen [BUN] and creatine kinase [CK]) and liver (aspartate transaminase [AST], alkaline phosphatase [ALP], and alanine transaminase [ALT]) toxicity were at normal levels in all cases except for ALP, which was within one standard deviation of the normal range and also high in the control mice (Fig. 6A). Blood electrolytes were all within the normal range except for phosphorus levels in the control group (Fig. 6B). Hematological analysis for white blood cell (WBC) count, red blood cell (RBC) count, % lymphocytes, % neutrophils, % monocytes, and % eosinophils showed similar behavior for all markers except for neutrophils, where the LGW01-08 formulated group was above the normal range. Notably, the WBC count was low for all groups including the control group (Fig. 6C). Of note, all values outside of the normal range were not statistically different from control values and/or were within one standard deviation of the normal range. Mice displayed normal, healthy weight gain during the 14-day monitoring period following subcutaneous administration (Fig. 6D). Additionally, stability data for freeze-dried 22% Pluronic solution was recorded for six months, confirming long-term stability of the formulated fluorophore (Fig. S3).

Vagus and recurrent laryngeal nerve (RLN) staining.

Mouse vagus nerves and rat RLN were stained with Pluronics formulated LGW01-08 using the optimized direct administration methodology to assess utility in a clinically relevant anatomical site. Administration of the nerve-specific probe for vagus nerves and RLN identification using the optimized hydrogel formulation was completed within 2 mins, representing a clinically viable approach that would fit within current thyroidectomy clinical workflows. Following staining, vagus nerves and RLNs were readily visualized lateral to the trachea using fluorescence imaging, but were largely unidentifiable using conventional white light visualization (Fig. 7A & 7C). Line profile quantification indicated the main identified vagus nerves in mice were sub-100 μm in diameter and calculated nerve SBRs for vagus nerves and RLN in rats demonstrated N/M ratios similar to the larger caliber sciatic and brachial plexus nerves imaged previously (Fig. 3, 7B & 7D). Additionally, quantified RLN to thyroid ratios were significantly greater than N/M ratios (n = 4 nerve sites, p=0.024, Fig.

7C), demonstrating the utility of Pluronics formulated LGW01-08 in RLN identification and visualization during thyroidectomy.

DISCUSSION

Clinically viable hydrogel-based formulations were evaluated to enable nerve-specific staining intraoperatively at the surgical site. Application of nerve-specific probes using this direct administration methodology would substantially reduce the required nerve-specific contrast agent dose, enabling clinical translation under an eIND.[65] However, liquid-based formulations are not ideal for this purpose as surgical sites routinely have irregular surfaces and steep angles that present challenges to direct application of liquid-based staining solution resulting in substantial pooling, non-specific background tissue uptake and diminished overall nerve contrast. To alleviate these difficulties, we designed and developed hydrogel-based formulation strategies, modeled after clinical gel and foam based formulations used as intraoperative hemostatic agents and surgical sealants,[62–64] to improve both application control and tissue staining penetration depth to faciliate buried nerve tissue visualization. Hydrogel-based formulations including Na Alginate and Pluronics were evaluated using our NIR nerve-specific fluorophore, LGW01-08 to develop a platform for robust and effective direct administration of nerve contrast during FGS.

A range of hydrogel formulations were screened *in vivo* using the previously optimized direct administration methodology.[48] Na Alginate at a concentration of 6.8% showed increased viscosity at 2 nM Ca^{+2} concentration, which is representative of the physiological levels of Ca^{+2} (~ 50-100 nM).[66] Moreover, 22% Pluronic gel displayed a gelation temperature of 33 °C (Fig. S1), which was ideal for the LGW01-08 application. The release kinetics studies of LGW01-08 from both gels showed a slow release over the experimental time. The overall slow release of LGW01-08 from both gels could be due to the interaction of this fluorophore with the hydrophobic portion of the polymers along with the high viscosity of the gels, where both factors can restrict the diffusion of the dye molecules across the gels matrix and thereby slow its rate of release.[67] No significant loss in nerve-specific fluorescence signal intensity or nerve SBRs vs. the liquid co-solvent formulation was observed except at the highest concentrations of each hydrogel (Fig. 1). The decrease in nerve-specific fluorescence intensity at the highest hydrogel concentrations (i.e., 8% Na Alginate and 25% Pluronics) was likely due to lower diffusion and tissue partition rates of LGW01-08 in these more solidified gels. The viscosity of the hydrogel concentration ranges were quantified by tissue spread at varying degrees of tilt to evaluate tissue hold and ease of application (Fig. 2). The optimal concentration of each hydrogel was selected (i.e., 6.5% Na Alginate and 22% Pluronics) based on both nerve-specific contrast vs. the co-solvent formulation and utility for application that facilitated tissue spread, but gelled rapidly upon application to minimize background staining. It was also determined that the unique gelling characteristics of Pluronics with increased temperature was ideal for application and subsequent tissue hold for the duration of staining in a large animal laparoscopic surgical model using the da Vinci surgical robot to assess its performance in an accurate clinical setting (Fig. 2C). Imaging during direct administration further highlighted the hydrogel formulation benefit of improved stain control on the vertical surface of the iliac plexus. The Pluronics formulation was easily applied and spread on the tissue as a liquid,

but immediately gelled upon contact and was subsequently held in place throughout the incubation process (Movie S2). Hydrogel formulation administration of LGW01-08 enabled fluorescence visualization of both exposed and buried nerve structures at the iliac plexus, which may have been enabled by the increased tissue penetration depth due to increased contact time vs. the liquid-based formulation.

While direct administration during surgery is potentially advantageous to limit overall dose, a rapid staining protocol is required to minimize disruption to the surgical workflow. The previously developed direct administration methodology required substantial washing time, resulting in a total tissue processing time of 12 minutes, which would be challenging to implement clinically. The hydrogel Pluronics formulation permitted improved control of the stained surfaces and thus we hypothesized that the overall tissue staining time could be vastly shortened without negatively affecting nerve contrast. Pluronics formulated LGW01-08 at varied concentrations (e.g., 200, 50, and 25 μg/mL) was used to stain murine nerve tissues for 1- or 5-minutes to assess the interplay between fluorophore concentration and incubation time (Fig. 3). The LGW01-08 concentrations were selected based on both the previously utilized 50 μg/mL optimal direct administration concentration using the co-solvent liquid formulation and the maximum dose that could be applied to fulfill microdose requirements for future eIND studies (i.e., 200 μg/mL).[48, 65] The 25 μg/mL concentration was tested to assess any improvements in nerve SBR from decreased dose as had been observed using the co-solvent direct administration strategy.[48] While no significant change in nerve contrast or SBR values were observed among the evaluated staining conditions, nerve signal intensities were positively correlated to changes in concentration and incubation time. Thus the 200 μg/mL concentration and 1 min incubation time were selected as ideal due to the tradeoff between the desire for a shortened staining protocol and maintained high nerve tissue signal intensity. Washing conditions were also evaluated to assess the shortest washing protocol that would result in maintained nerve tissue fluorescence intensity and SBR, where washing resulted in a steady increase in nerve intensity values and SBRs values for up to six washes. We hypothesize that this increased nerve signal was due to the washing process resolubilizing fluorophore in the wash solutions and allowing for further diffusion into the nerve tissue, while improvements in nerve SBRs likely represent further removal of nonspecifically bound fluorophore from surrounding tissues. Further washing only showed marginal improvement in nerve tissue intensity and overall SBR, resulting in an optimized staining protocol with six washes (i.e., rapid flushes of the stained tissue surface) bringing the overall staining protocol time to 1-2 minutes depending on the required time to complete tissue flushing. Tissue clearance assessment saw no loss in nerve signal and slight increases in nerve SBRs for up to 30 min after washing completions, suggesting that no significant loss in nerve signal or SBRs will occur during the course of a variety of typical surgical nerve sparing procedures (Fig. 4).

Staining depth penetration will be vital to successful direct administration of nerve-specific probes to provide guidance as surgeons dissect near highly innervated sites. Pluronics stained tissue diffusion profiles were modeled permitting calculation of the diffusion coefficient,[68] which allowed prediction of the optimized direct administration methodology to stain nerve tissue at up to 0.5-1 mm depths where increased incubation times increase staining penetration (Fig. 5). Thus, the optimized direct administration

methodology provides a flexible platform for nerve tissue staining intraoperatively, where incubation times can be adjusted to permit visualization of nerves at various depths. During thyroidectomy the RLN is most often identified at its point of laryngeal entry, where the nerve is buried beneath ~0.5–1 mm of tissue.[69] Therefore, the optimized hydrogel formulation and direct administration methodology yield adequate penetration, that can be increased via increased incubation time, for RLN staining and visualization during thyroidectomy. Additionally, modeling nerve staining depth facilitates assessment of the utility for additional surgical indications. For example, during nerve-sparing prostatectomy the vital cavernous nerves can be buried beneath 0.3–1 mm of tissue, suggesting that the developed hydrogel formulation and direct administration methodology could also provide utility for this procedure.[70]

Preclinical pharmacology and toxicology testing in rodents, including blood pharmacology, behavioral assessment, necropsy and histological analysis of each tissue 14-days after administration is required for a successful eIND application.[65] Initial toxicology studies of the Pluronics formulated LGW01-08 were completed at ~100x the body surface area scaled human microdose (Fig. 6). All blood markers for Pluronics formulated LGW01-08 injected animals were either within the normal range or equivalent to control uninjected and vehicle injected animals. Additionally, all mice demonstrated healthy weight gain over the study period, providing confidence to continue towards clinical translation. Further validation of the utility of the optimized direct administration methodology was provided by mouse vagus and rat RLN staining, where vagus nerves with sub-100 μm diameters were clearly visible in mice and RLN tissue was highlighted alongside branching vagus nerves in rats with high contrast over thyroid tissue (Fig. 7). These results show the advantages of nerve specific FGS, where nerve tissue was readily visualized with high resolution and specificity in real-time, while conventional white light guided nerve visualization was challenging. Furthermore, these studies demonstrate that the optimized Pluronics formulation provided the necessary delivery of nerve-specific fluorophore to the nerves of interest for thyroidectomy, which were clearly visible over neighboring anatomy including muscle, fascia, adipose, and thyroid tissues. Scaling of these studies to large animal or cadaver studies would provide further validation in more accurate surgical models and will be the focus of future studies.

Through systematic optimization and characterization of hydrogel and fluorophore concentrations, staining incubation time and washing protocol, an optimized direct administration methodology using a hydrogel-based formulation was developed herein that provides bright, nerve-specific staining that can be applied to many tissue shapes, tilts, and morphologies in <2 min. The unique physical characteristics of the Pluronics-based formulation allow for nerve-specific stain solution to be applied with relative ease as a liquid and then remain in place following near instantaneous gel formation. The resulting administration platform provides a clinically viable method for fluorescence guided nerve-sparing during thyroidectomy as well as other procedures and an improved route for rapid clinical translation under eIND regulations, speeding the path to clinical translation.

MATERIALS & METHODS

Nerve-specific contrast agents and formulations.

Oxazine 4 was purchased from Exciton (Lockboume, OH) and used without further purification. The synthesis, purification and characterization of LGW01-08 has been previously published.[45] The previously used co-solvent formulation containing 10% DMSO, 5% Kolliphor EL, 65% serum, and 20% phosphate buffered saline (PBS) was used for comparison to the hydrogel-based sodium alginate (Na Alginate) and F-127 Pluoronics (Pluronics) formulations presented herein.[24, 48, 71] Pluronics/poloxamers are FDA approved poly(ethylene oxide)/poly(propylene oxide)/poly(ethyleneoxide) (PEO-PPO-PEO) triblock copolymers, aqueous solutions of which undergo sol-to-gel transition with increasing temperature above a lower critical gelation temperature.[59–61] Pluronics F-127 (Letco Medical, Decatur, AL) was added to cold water (4-10 °C) to achieve 20, 22, and 25% (w/v) F-127 hydrogel concentration. The solutions were left overnight on a shaker in the cold room, to ensure complete solubilization of the polymer. Alginates have been used as versatile bio-polymers and have a unique property of gelling in the presence of divalent ions such as calcium. 5%, 6.5% and 8% (w/v) alginate gels were prepared by dissolving Na Alginate (Sigma Aldrich, St. Louis, MO) in water at 60 °C for 2-3 h on a shaker to ensure complete wetting and solubilization of the alginate. To load the LGW01-08 fluorophore into the polymer solution, the fluorophore stock solution was prepared in DMSO; a specific volume of the stock solution was spiked into the polymer solution resulting in the targeted final fluorophore concentration (range of 50-100 μg/mL), The final concentration of DMSO in the polymer solution was less than 1% (v/v). To quantify the LGW01-08 in the polymer solution before gelation a liquate of the solution was diluted into Acetonitrile and the concentration was measure by high-performance liquid chromatography (HPLC) as detailed below.

Rheological measurements were performed on a AR2000 rheometer (TA instruments, Texas). The polymer solution was placed between parallel plate geometry of 25 mm diameter and a Peltier heat pump. The loading gap was set at 1 mm. Temperature dependent viscosity change was measured from 10-60 °C at a heating rate of 1 °C/min and a controlled shear rate of 0.1 s^{-1}.

Release kinetics studies were performed after loading LGW01-08 into Na Alginate or Pluronic F127 by a previously described simple mixing method.[67] Briefly, a solution of LGW01-08 at 0.2 mg/mL was prepared in Pluronic F127 (22% wt), where 1 mL was loaded into a 15 mL tube (n=4) and the temperature was increased to 37 °C resulting in gel formation. Similarly, a solution of LGW01-08 at 0.2 mg/mL was prepared in Na Alginate at (6.5% wt), where a volume of 1 mL of the solution was loaded into 15 mL tube (n=4), which was converted to a gel through the addition of calcium chloride. Ten minutes post gel formation, 14 mL of phosphate buffer saline (1X, pH 7.4) pre-warmed to 37 °C was added at the top of the gel matrix in the 15 mL tube. The tube was then placed into a shaker bath adjusted to 50 rpm and the temperature set to 37 °C to quantify the drug release. Samples of 0.5 mL were withdrawn from Na Alginate gel tubes at 0.5, 2, 4, 6, 24, 48, 72, 96, 120.5, 144, 168 and 192 h and from the Pluronic F127 gel tubes at 0.5, 2, 4, 6, 24,

48, 72, 96, 120.5, 144, 168,192, 216, 214 and 276 h time intervals. A 0.5 mL volume of the fresh PBS buffer replaced the samples in the tubes drawn at the respective time points. All measurements were performed in quadruplicate. The cumulative percent drug release was determined by HPLC as described below. During the experiment, the integrity of the gel for all samples was monitored visually. The LGW01-08 concentration in the Pluronics F127 and Na Alginate gels was measured using a Shimadzu HPLC system with an LC-20 AT pump, an SPD M20 and a photodiode array detector (Shimadzu, Kyoto, Japan). The LGW01-08 concentration was quantified on a Zorbax C18 Column (4.6×75 mm, 3.5 μm) using isocratic mode with acetonitrile/water (55/45 mixing ratio) containing 1% methanol and 0.1% phosphoric acid. The mobile phase flow rate was 1 mL/min, and the injection volume was 10 μL. The column temperature was maintained at 40 °C. The Photodiode Array detector detected the LGW01-08 peaks at 632 nm. The retention time for LGW01-08 was at 0.83 min. The release profiles for LGW01-08 from both gels were fitted to a two-phase exponential association model (Graph-Pad Prism Version 7.03 for Windows).

Freshly prepared LGW01-08 fluorophore solution (50 μg/mL) in Pluronics 127 at 22% was loaded at 10 mL into a Wheaton® Vacule® 100 mL vials. The vials were placed in a shelf freeze-dryer, FreeZone® Triad™ Freeze Dry System, Labconco, (Kansas City, MO). The freeze-drying cycle consisted of; Prefreeze Segment, vials froze at −80 °C for 6 h. Segment 1, primary drying, ramp 4 °C/min, hold −55 °C for 24 h. Segment 2, secondary drying, ramp 5 °C/min, hold - 5 °C for 12 h. Segment 3, holding, ramp 0.01 °C/min, hold 0 °C for 5 h and the last step in the cycle was ramp 0.01 °C/min, hold at 4 °C. At the end of the cycle, the vials were filled with argon and stoppered for storage. The vials were stored for up to six months at 4 °C. To quantify the loading of LGW01-08 in the lyophilized samples, the freeze-dried powder was rehydrated with cold water (10 °C) and the solution was filtered with 0.45 μm syringe filter. LGW01-08 concentration was quantified using a fluorometer, where the intensity of the solution was measured at E_x/E_m 602/635 nm.

Animals.

Approval for the use of all animals in this study was obtained from the appropriate Institutional Animal Care and Use Committee (IACUC). Male CD-1 mice (Charles River Laboratories, Wilmington, MA) weighing 22-24g were anaesthetized prior to surgery with 100 mg/kg ketamine and 10 mg/kg xylazine (Patterson Veterinary, Devens, MA) administered intraperitoneally (IP). Full depth of anesthesia was assessed using the toe pinch method for reactivity prior to all surgical procedures. At the completion of all studies, mice were euthanized using inhalation of carbon dioxide followed by cervical dislocation. Female swine (Pork Power, Springfield, IL) weighing 60-70 kg were anaesthetized with 4% isoflurane. At the completion of all studies, swine were euthanized by intravenous administration of Euthasol (Virbac, Fort Worth, TX).

In mice and rats the brachial plexus, sciatic, vagus and recurrent laryngeal nerves were surgically exposed by removal of overlaying adipose and muscle tissues for direct administration of LGW01-08 to the exposed nerve and surrounding tissues. In swine the bowel was exposed via lateral peritoneal incision and gently removed from the body cavity for hydrogel formulation assessment. For laparoscopic studies, the da Vinci Si Surgical

System was docked to the peritoneal space and iliac nerve sites were surgical exposed by removal of overlaying lymph node and adipose tissue.

Gel formulation and viscosity screening.

Each novel hydrogel-based formulation was tested in mice using the direct administration methodology developed using the liquid based co-solvent formulation.[48] LGW01-08 was formulated in 5.0, 6.5, and 8.0% Na Alginate as well as 20, 22, and 25% Pluronics at 50 μg/mL concentration. Each exposed brachial plexus and sciatic nerve site was incubated with the formulated fluorophore for five min, followed by nine flushes with PBS, a secondary five min incubation with blank (i.e., unloaded) formulation, and nine additional flushes with PBS to remove non-specifically bound fluorophore. Fluorescence and color images were acquired immediately following staining and 30 min following staining to observe improvements in nerve SBRs due to clearance. Nerve sites were stained with LGW01-08 in the previously utilized co-solvent formulation using the same direct administration methodology as positive controls and unstained nerve sites were imaged as negative controls (n=3 mice or n=6 nerve sites [50/50 brachial plexus / sciatic nerve] per staining condition).[24, 36, 48]

To determine the optimal amount of hydrogel for each formulation, oxazine 4 at 400 μg/mL in 5.0, 6.5, and 8.0% Na Alginate as well as 20, 22, and 25% Pluronics was dropped onto swine intestinal tissue that had been shimmed to 0, 35, and 65° angles. A 1 mL pipette was used to apply 300 μL of each formulation to porcine small intestine held on an angled shim. The small intestine was kept at internal body temperature and only removed externally for testing the formulation. A new section of small intestine was used to test each hydrogel formulation. All small intestine regions were gently wiped with medical gauze to remove any noticeable serous fluid prior to formulation application. A color photograph was taken 30 seconds after direct formulation application for surface area analysis using ruler measurements on the tissue shims adjacent to the tissue. All formulations were tested in triplicate on the spine bowel. Surface area measurements were used to quantify the tissue spread and administration control characteristics.

Large animal nerve staining.

To validate the viscosity and performance of the novel gel formulations in a clinically relevant surgical model, the gel formulation was applied laparoscopically to the swine iliac plexus using a da Vinci Si surgical robotic system (Intuitive Surgical, Sunnyvale, CA). The direct administration gel and liquid formulation protocols were used to stain the swine iliac plexus as well as the surrounding muscle and adipose tissue with 400 μg/mL oxazine 4 solubilized in the co-solvent, 22% Pluronics or 6.5% Na Alginate formulations. Color and fluorescence video were acquired during as well as one hour after staining.

Direct administration protocol optimization.

The nerve-specific fluorophore concentration, incubation time, and washing protocols were optimized for the selected hydrogel formulation. 25, 50, and 200 μg/mL concentrations of LGW01-08 at 1- and 5-minute incubation times in 22% Pluronics were used to stain murine brachial plexus and sciatic nerve sites followed by 18 PBS flushes (n = 6 nerve sites [50/50

brachial plexus / sciatic nerve] per staining condition). Images were collected following each flush step for six washes and then every three washes out to 18 washes. Washing was completed using PBS stored at 4 °C to evaluate the utility of chilled PBS to liquify the gelled Pluronics solution vs. room temperature 20-25 °C PBS. Washes consisted of a short flush of PBS followed immediately by removal using absorption with gauze.

Direct administration tissue penetration.

22% Pluronics formulated LGW01-08 was used to stain murine muscle tissue *in vivo* prior to resection using the optimized washing protocol of six washes of room-temperature PBS. The stained muscle tissue was immediately removed and flash frozen in optimal cutting temperature (OCT) compound (Thermo Fisher Scientific, Waltham, MA). Muscle tissue was cryosectioned at 10 μm thickness in cross section (n=3 sections) for imaging using an AxioObserver inverted microscope (Carl Zeiss AG, Oberkochen, Germany). A Photofluor II light source (89 North, Burlington, VT) was filtered with a 620 ± 30 nm bandpass excitation filter and fluorescence images were collected using a 700 ± 37.5 nm emission filter on an Axiocam 506 camera (Zeiss). All filters were obtained from Chroma Technology (Bellows Falls, VT). Images were captured with camera exposure times ranging from 0.5 – 1 sec at 10X magnification. Tissue penetration was analyzed using line profiles generated in ImageJ using the plot profile function. Three line profiles were generated per tissue section, where the width of the line used to generate the profile was 10 pixels. Analysis of standard deviation in the median as a function of increasing line width found the 10-pixel width as the narrowest line width at which standard deviations leveled off, enabling quantification of fluorescence intensity line profiles with high precision and accuracy. The average line profile was used to calculate diffusion coefficient using the mathematical model developed by Kang *et. al.* deployed using MatLab (The MathWorks, Natick, MA).[68] The fluorophore detection limit was identified by placing microcentrifuge tubes containing a range of concentrations of LGW01-08 in PBS beneath 1 mm of muscle tissue. Muscle tissue was resected from the mouse peritoneum and measured with calipers to ensure consistent depth. Fluorescence intensities were quantified via region of interest analysis and normalized to the background autofluorescence of the muscle via subtraction. The lowest concentration that could be detected above the background signal (>0 A.U. after background subtraction) was chosen as the detection limit.

Toxicity testing.

Two cohorts of mice per were subcutaneously administered either 0.5 mL 22% Pluronics loaded with LGW01-08 for a dose of 1.8 mg/kg or control unloaded 22% Pluronics for blood chemistry analysis and 14-day weight monitoring studies (n=5 mice per cohort per formulation). The dose was calculated based on body surface area scaling between mice and humans (12.3 scaling factor) to be 100x the maximum dose allowed for human microdose studies (100 μg).[72] Blood chemistry cohort mice were euthanized 24 hours following systemic administration and blood was collected into lithium heparin tubes via cardiac puncture. Blood was sent to IDEXX laboratory (Veterinary Diagnostic, Portland, OR) for standard blood chemistry analysis. The blood markers evaluated include blood urea nitrogen (BUN), creatinine kinase (CK), alanine transaminase (ALT), aspartate transaminase (AST), and alkaline phosphatase (ALP). Hematological analysis of white blood cell (WBC)

count, red blood cell (RBC) count, Hematocrit (HC), % neutrophils, % lymphocyte, % monocyte, % eosinophil, and % basophile was performed. The electrolytes assessed include phosphorus, calcium, sodium, potassium, and chloride. The weight monitoring cohort mice were weighed 1-, 4-, 6-, 8-, 10-, 11-, and 14-days following administration.

Vagus and Recurrent Laryngeal Nerve Staining.

To evaluate the clinical utility of the optimized hydrogel formulation and direct administration methodology, murine and rat trachea, thyroid, vagus nerve, RLN and surrounding tissue was exposed following resection of the salivary gland and dissection of the overlaying muscle tissue (n = 4 nerve sites per species). LGW01-08 formulated in 22% Pluronics at a concentration of 200 μg/mL was incubated on the entire exposed tissue area for 1 min, followed by six PBS flushes. Images were acquired for up to 30 minutes following direct administration.

Intraoperative fluorescence imaging systems.

A custom-built small animal imaging system capable of real-time color and fluorescence imaging was used to acquire *in vivo* murine images.[71] Briefly, the imaging system consisted of a QImaging EXi Blue monochrome camera (Surrey, British Columbia, CA) for fluorescence detection with a removable Bayer filter for collecting co-registered color and fluorescence images. A PhotoFluor II light source (89 North, Burlington, VT) was focused onto the surgical field through a liquid light guide and used unfiltered for white light illumination. For fluorescence excitation, the PhotoFluor II was filtered with a 620 ± 30 nm bandpass excitation filter. Resulting fluorescence was collected with a 700 ± 37.5 nm bandpass emission filter for image collection. All filters were obtained from Chroma Technology (Bellows Falls, VT). Camera exposure times ranged from 10 – 2000 ms for fluorescence image collection.

A custom-built laparoscopic imaging system also capable of real-time color and fluorescence imaging was used to acquire *in vivo* swine images. The imaging system was integrated into the da Vinci Si surgical system (Intuitive Surgical, Sunnyvale, CA) and consisted of a Necsel Neon 5W 640 nm laser (Necsel, Milpitas, CA) coupled to the da Vinci Si endoscope with a Semrock 642 nm StopLine single-notch blocking filter (Semrock, Rochester, NY) to remove excitation light from the acquired fluorescence images. The 642 nm StopLine blocking filter was placed in the Si camera sterile adaptor between the rod lens endoscope and the Si camera head. Fluorescent signal acquisition occurred in the Si white light mode with the blocking filter removing the 642 nm excitation light and the fluorescent signal detected primarily on the RGB red-Bayer elements. Laser power at the endoscope tip measured 800 mW with optical power loses occurring primarily at the laser fiber/light guide and the Si camera head/rod lens interfaces. Fluorescence and color videos were captured using the Si Vision Side Cart at an exposure time of 2 ms. Images were taken from screen captures of the *in vivo* video clips. Videos were recorded on a Panasonic SDI recorder connected to the TilePro video out connections on da Vinci Si Vision Side Cart.

Intraoperative nerve image analysis.

Custom written MatLab code was used to analyze the tissue specific fluorescence where regions of interest were selected using the white light images. These regions of interest were then analyzed on the co-registered matched fluorescence images permitting quantification of the mean tissue intensities and nerve to muscle (N/M), nerve to adipose (N/A), and nerve to cut muscle (N/CM) ratios. Intensity measurements were divided by the exposure time to obtain normalized intensity per second measurements. For vagus and RLN staining image analysis, fluorescent line profiles were generated in ImageJ using the plot profile function. Line profiles were background and exposure time corrected. Thyroid intensities were calculated via region of interest analysis and used to calculated nerve to thyroid (N/T) ratios.

Statistical analysis.

Significant differences between quantified means were evaluated using a one-way ANOVA followed by a Fisher's LSD multiple comparison test with no assumption of sphericity using the Geisser-Greenhouse correction to compare all mean nerve signal intensities and nerve to background tissue ratios. The α value was set to 0.05 for all analyses. Results were presented as mean ± standard deviation (S.D.). All statistical analysis was performed using GraphPad Prism (La Jolla, CA).

Supplementary Material

Refer to Web version on PubMed Central for supplementary material.

ACKNOWLEDGEMENTS

We would like to thank Xiaochun Xu and Kenneth Tichauer for experimental assistance, data analysis support, and insightful discussions. This work was funded by the National Institute of Biomedical Imaging and Bioengineering (R01EB021362).

REFERENCES

1. Hall MJ, DeFrances CJ, Williams SN, Golosinskiy A & Schwartzman A National Hospital Discharge Survey: 2007 summary. Natl Health Stat Report, 1-20, 24 (2010).
2. Walsh PC & Donker PJ Impotence following radical prostatectomy: insight into etiology and prevention. J Urol 128, 492–497 (1982). [PubMed: 7120554]
3. Ficarra V et al. Systematic review and meta-analysis of studies reporting urinary continence recovery after robot-assisted radical prostatectomy. Eur Urol 62, 405–417 (2012). [PubMed: 22749852]
4. Damber JE & Khatami A Surgical treatment of localized prostate cancer. Acta Oncol 44, 599–604 (2005). [PubMed: 16165919]
5. Rawla P Epidemiology of Prostate Cancer. World J Oncol 10, 63–89 (2019). [PubMed: 31068988]
6. Hammer A et al. Global epidemiology of hysterectomy: possible impact on gynecological cancer rates. Am J Obstet Gynecol 213, 23–29 (2015). [PubMed: 25724402]
7. Kingsnorth A & LeBlanc K Hernias: inguinal and incisional. Lancet 362, 1561–1571 (2003). [PubMed: 14615114]
8. Francis DO, Randolph G & Davies L Nationwide Variation in Rates of Thyroidectomy Among US Medicare Beneficiaries. JAMA Otolaryngol Head Neck Surg 143, 1122–1125 (2017). [PubMed: 29049468]

9. Swonke ML, Shakibai N & Chaaban MR Medical Malpractice Trends in Thyroidectomies among General Surgeons and Otolaryngologists. OTO Open 4, 2473974X20921141 (2020).
10. Christou N & Mathonnet M Complications after total thyroidectomy. Journal of Visceral Surgery 150, 249–256 (2013). [PubMed: 23746996]
11. Zakaria Recurrent Laryngeal Nerve Injury in Thyroid Surgery. Oman Medical Journal 26, 34–38 (2011). [PubMed: 22043377]
12. Abadin SS, Kaplan EL & Angelos P Malpractice litigation after thyroid surgery: The role of recurrent laryngeal nerve injuries, 1989–2009. Surgery 148, 718–723 (2010). [PubMed: 20709343]
13. Al-Qurayshi Z, Robins R, Hauch A, Randolph GW & Kandil E Association of Surgeon Volume With Outcomes and Cost Savings Following Thyroidectomy. JAMA Otolaryngology–Head & Neck Surgery 142 (2016).
14. Saunders BD et al. Who performs endocrine operations in the United States? Surgery 134, 924–931 (2003). [PubMed: 14668724]
15. Higgins TS et al. Recurrent laryngeal nerve monitoring versus identification alone on post-thyroidectomy true vocal fold palsy: A meta-analysis. The Laryngoscope 121, 1009–1017 (2011). [PubMed: 21520117]
16. Shao T, Qiu W & Yang W Anatomical variations of the recurrent laryngeal nerve in Chinese patients: a prospective study of 2,404 patients. Scientific Reports 6 (2016).
17. Feng AL et al. Increased prevalence of neural monitoring during thyroidectomy: Global surgical survey. The Laryngoscope (2019).
18. Hartl DM et al. Ultrasound visualization of the vagus nerve for intraoperative neuromonitoring in thyroid surgery. Eur Radiol 31, 4063–4070 (2021). [PubMed: 33241516]
19. Drakonaki E et al. Normal anatomy, variants and factors associated with the cervical vagus nerve topography: a high-resolution ultrasound study. Surg Radiol Anat 43, 1753–1764 (2021). [PubMed: 34524485]
20. Ning B et al. Improved Nerve Visualization in Head and Neck Surgery Using Mueller Polarimetric Imaging: Preclinical Feasibility Study in a Swine Model. Lasers Surg Med 53, 1427–1434 (2021). [PubMed: 34036583]
21. Sakata LM, Deleon-Ortega J, Sakata V & Girkin CA Optical coherence tomography of the retina and optic nerve - a review. Clin Exp Ophthalmol 37, 90–99 (2009). [PubMed: 19338607]
22. AV DS, Lin H, Henderson ER, Samkoe KS & Pogue BW Review of fluorescence guided surgery systems: identification of key performance capabilities beyond indocyanine green imaging. J Biomed Opt 21, 80901 (2016). [PubMed: 27533438]
23. Ashitate Y, Stockdale A, Choi HS, Laurence RG & Frangioni JV Real-time simultaneous near-infrared fluorescence imaging of bile duct and arterial anatomy. J Surg Res 176, 7–13 (2012). [PubMed: 21816414]
24. Gibbs-Strauss SL et al. Nerve-highlighting fluorescent contrast agents for image-guided surgery. Mol Imaging 10, 91–101 (2011). [PubMed: 21439254]
25. Gotoh K et al. A novel image-guided surgery of hepatocellular carcinoma by indocyanine green fluorescence imaging navigation. J Surg Oncol 100, 75–79 (2009). [PubMed: 19301311]
26. Hirche C et al. An experimental study to evaluate the Fluobeam 800 imaging system for fluorescence-guided lymphatic imaging and sentinel node biopsy. Surg Innov 20, 516–523 (2013). [PubMed: 23275469]
27. Kitagawa H et al. Visualization of the Stomach's Arterial Networks During Esophageal Surgery Using the HyperEye Medical System. Anticancer Res 35, 6201–6205 (2015). [PubMed: 26504051]
28. Lee BT et al. The FLARE intraoperative near-infrared fluorescence imaging system: a first-in-human clinical trial in perforator flap breast reconstruction. Plastic and reconstructive surgery 126, 1472–1481 (2010). [PubMed: 21042103]
29. Mannoh EA, Parker LB, Thomas G, Solorzano CC & Mahadevan-Jansen A Development of an imaging device for label-free parathyroid gland identification and vascularity assessment. J Biophotonics 14, e202100008 (2021). [PubMed: 33583122]

30. Thomas G et al. Comparing intraoperative parathyroid identification based on surgeon experience versus near infrared autofluorescence detection - A surgeon-blinded multicentric study. Am J Surg (2021).
31. Troyan SL et al. The FLARE intraoperative near-infrared fluorescence imaging system: a first-in-human clinical trial in breast cancer sentinel lymph node mapping. Annals of surgical oncology 16, 2943–2952 (2009). [PubMed: 19582506]
32. Tummers QR et al. Real-time intraoperative detection of breast cancer using near-infrared fluorescence imaging and Methylene Blue. Eur J Surg Oncol 40, 850–858 (2014). [PubMed: 24862545]
33. Verbeek FP et al. Intraoperative near infrared fluorescence guided identification of the ureters using low dose methylene blue: a first in human experience. J Urol 190, 574–579 (2013). [PubMed: 23466242]
34. Wu C et al. Molecular probes for imaging myelinated white matter in CNS. J Med Chem 51, 6682–6688 (2008). [PubMed: 18844339]
35. Wang C et al. In situ fluorescence imaging of myelination. J Histochem Cytochem 58, 611–621 (2010). [PubMed: 20354147]
36. Gibbs SL et al. Structure-activity relationship of nerve-highlighting fluorophores. PLoS One 8, e73493 (2013). [PubMed: 24039960]
37. Stankoff B et al. Imaging of CNS myelin by positron-emission tomography. Proc Natl Acad Sci U S A 103, 9304–9309 (2006). [PubMed: 16754874]
38. Cotero VE et al. Intraoperative fluorescence imaging of peripheral and central nerves through a myelin-selective contrast agent. Mol Imaging Biol 14, 708–717 (2012). [PubMed: 22488576]
39. Cotero VE et al. Improved Intraoperative Visualization of Nerves through a Myelin-Binding Fluorophore and Dual-Mode Laparoscopic Imaging. PLoS One 10, e0130276 (2015). [PubMed: 26076448]
40. Bajaj A et al. Identification of the protein target of myelin-binding ligands by immunohistochemistry and biochemical analyses. J Histochem Cytochem 61, 19–30 (2013). [PubMed: 23092790]
41. Gibbs-Strauss SL et al. Molecular imaging agents specific for the annulus fibrosus of the intervertebral disk. Mol Imaging 9, 128–140 (2010). [PubMed: 20487679]
42. Meyers JR et al. Lighting up the senses: FM1-43 loading of sensory cells through nonselective ion channels. J Neurosci 23, 4054–4065 (2003). [PubMed: 12764092]
43. Wang C et al. Longitudinal near-infrared imaging of myelination. J Neurosci 31, 2382–2390 (2011). [PubMed: 21325505]
44. Park MH et al. Prototype nerve-specific near-infrared fluorophores. Theranostics 4, 823–833 (2014). [PubMed: 24955143]
45. Wang LG et al. Near-infrared nerve-binding fluorophores for buried nerve tissue imaging. Sci Transl Med 12 (2020).
46. Barth CW et al. Clinically translatable formulation strategies for systemic administration of nerve-specific probes. Adv Ther (Weinh) 4 (2021).
47. Tummers WS et al. Regulatory Aspects of Optical Methods and Exogenous Targets for Cancer Detection. Cancer Research 77, 2197–2206 (2017). [PubMed: 28428283]
48. Barth CW & Gibbs SL Direct Administration of Nerve-Specific Contrast to Improve Nerve Sparing Radical Prostatectomy. Theranostics 7, 573–593 (2017). [PubMed: 28255352]
49. Gelderblom H, Verweij J, Nooter K & Sparreboom A Cremophor EL: the drawbacks and advantages of vehicle selection for drug formulation. Eur J Cancer 37, 1590–1598 (2001). [PubMed: 11527683]
50. Gallo E et al. Systematic overview of soft materials as a novel frontier for MRI contrast agents. RSC Advances 10, 27064–27080 (2020).
51. Wu X et al. Injectable and thermosensitive hydrogels mediating a universal macromolecular contrast agent with radiopacity for noninvasive imaging of deep tissues. Bioactive Materials 6, 4717–4728 (2021). [PubMed: 34136722]

52. Lock LL et al. One-Component Supramolecular Filament Hydrogels as Theranostic Label-Free Magnetic Resonance Imaging Agents. ACS Nano 11, 797–805 (2017). [PubMed: 28075559]
53. . Cho S-H et al. Photothermal-modulated drug delivery and magnetic relaxation based on collagen/poly(γ-glutamic acid) hydrogel. International Journal of Nanomedicine Volume 12, 2607–2620 (2017). [PubMed: 28408827]
54. Lee KY & Mooney DJ Alginate: properties and biomedical applications. Prog Polym Sci 37, 106–126 (2012). [PubMed: 22125349]
55. Bouhadir KH, Alsberg E & Mooney DJ Hydrogels for combination delivery of antineoplastic agents. Biomaterials 22, 2625–2633 (2001). [PubMed: 11519782]
56. Shah VM, Nguyen DX, Rao DA, Alany RG & Alani AWG in Temperature-Responsive Polymers 313–327 (2018).
57. Rassing J & Attwood D Ultrasonic velocity and light-scattering studies on the polyoxyethylene—polyoxypropylene copolymer Pluronic F127 in aqueous solution. International Journal of Pharmaceutics 13, 47–55 (1982).
58. Cook MT, Haddow P, Kirton SB & McAuley WJ Polymers Exhibiting Lower Critical Solution Temperatures as a Route to Thermoreversible Gelators for Healthcare. Adv Func Materials 31, 2008123 (2021).
59. Nie S, Hsiao WL, Pan W & Yang Z Thermoreversible Pluronic F127-based hydrogel containing liposomes for the controlled delivery of paclitaxel: in vitro drug release, cell cytotoxicity, and uptake studies. Int J Nanomedicine 6, 151–166 (2011). [PubMed: 21499415]
60. Diniz IM et al. Pluronic F-127 hydrogel as a promising scaffold for encapsulation of dental-derived mesenchymal stem cells. J Mater Sci Mater Med 26, 153 (2015). [PubMed: 25773231]
61. Suntornnond R, Tan EYS, An J & Chua CK A highly printable and biocompatible hydrogel composite for direct printing of soft and perfusable vasculature-like structures. Sci Rep 7, 16902 (2017). [PubMed: 29203812]
62. Stolzenburg J-U et al. Hemostasis during nerve-sparing endoscopic extraperitoneal radical prostatectomy. Journal of endourology 24, 505–509 (2010). [PubMed: 19619063]
63. Liatsikos EN, Katsakiori P & Stolzenburg J-U in Endoscopic Extraperitoneal Radical Prostatectomy 135–142 (Springer, 2007).
64. Unosson J, Montufar EB, Engqvist H, Ginebra MP & Persson C Brushite foams--the effect of Tween(R) 80 and Pluronic(R) F-127 on foam porosity and mechanical properties. J Biomed Mater Res B Appl Biomater 104, 67–77 (2016). [PubMed: 25615405]
65. .(ed. F.a.D. A. US Department of Health and Human Services, Center for Drug Evaluation and Research) (Washington DC, USA; 2006).
66. Breitwieser GE Extracellular calcium as an integrator of tissue function. Int J Biochem Cell Biol 40, 1467–1480 (2008). [PubMed: 18328773]
67. Mishra GP, Kinser R, Wierzbicki IH, Alany RG & Alani AW In situ gelling polyvalerolactone-based thermosensitive hydrogel for sustained drug delivery. Eur J Pharm Biopharm 88, 397–405 (2014). [PubMed: 24931340]
68. Kang S et al. Modeling the binding and diffusion of receptor-targeted nanoparticles topically applied on fresh tissue specimens. Physics in Medicine & Biology 64 (2019).
69. Fundakowski CE et al. Surgical management of the recurrent laryngeal nerve in thyroidectomy: American Head and Neck Society Consensus Statement. Head & Neck 40, 663–675 (2018). [PubMed: 29461666]
70. Tewari A et al. An Operative and Anatomic Study to Help in Nerve Sparing during Laparoscopic and Robotic Radical Prostatectomy. European Urology 43, 444–454 (2003). [PubMed: 12705985]
71. Hackman KM et al. Polymeric Micelles as Carriers for Nerve-Highlighting Fluorescent Probe Delivery. Mol Pharm 12, 4386–4394 (2015). [PubMed: 26485440]
72. Nair AB & Jacob S A simple practice guide for dose conversion between animals and human. J Basic Clin Pharm 7, 27–31 (2016). [PubMed: 27057123]

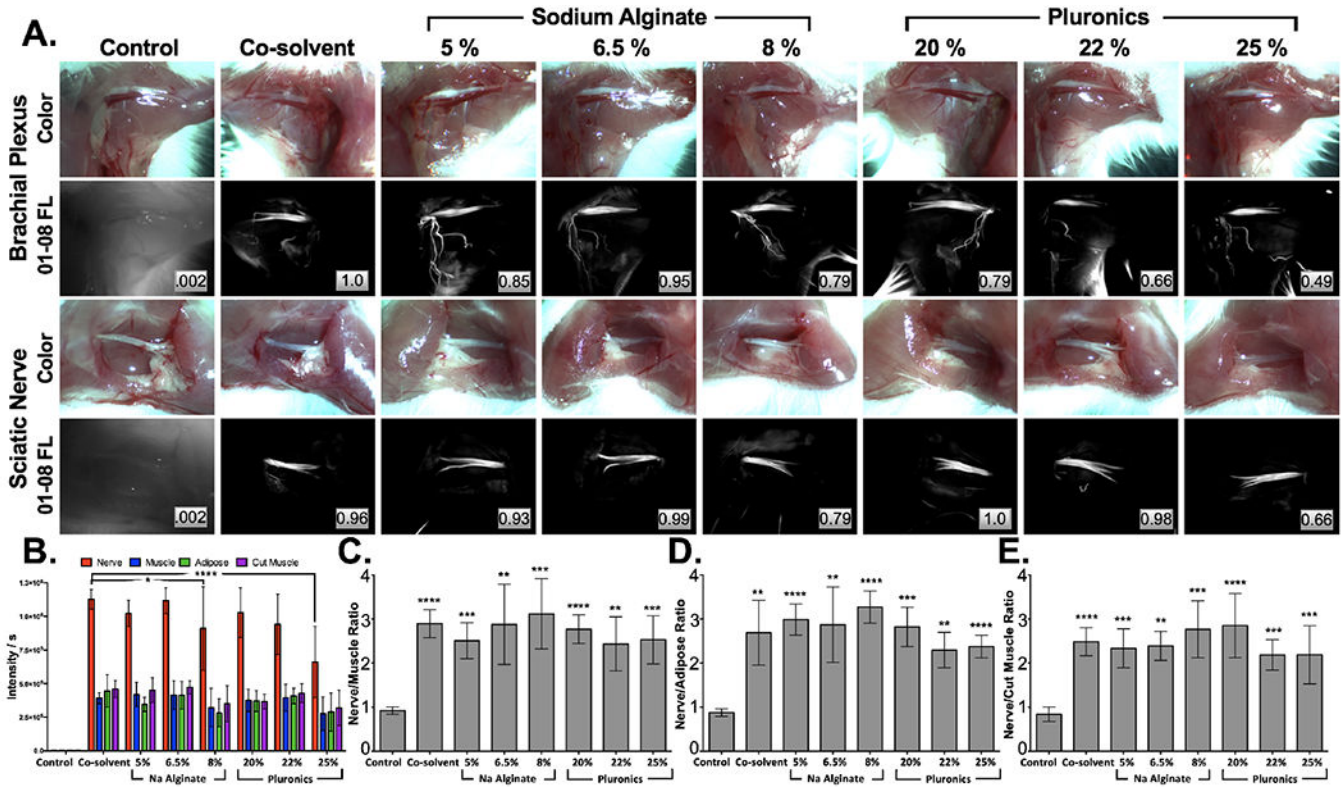

Figure 1: Hydrogel-based formulation screening.

A. Representative murine brachial plexus (top) and sciatic nerve (bottom) images were used to **B.** quantify tissue intensities, enabling calculation of **C.** nerve to muscle **D.** nerve to adipose and **E.** nerve to cut muscle SBRs stained with 50 μg/mL LGW01-08 in each concentration of Na Alginate and Pluronics hydrogel formulations vs. the co-solvent formulation. All images are representative of data collected for n=6 nerve sites per formulation. Images are displayed without normalization. Inset boxes show intensity metrics denoting the fraction of the brightest fluorescence intensity that the image represents between images in the same row. All quantified data is presented as mean +/− standard deviation. FL = fluorescence. Nerve intensity data for each formulation was compared to the co-solvent formulation data to test for significance. Nerve SBR data for each formulation was compared to control unstained data to test for significance. * = p value < 0.05, ** = p value < 0.01, *** = p value < 0.001, **** = p value < 0.0001.

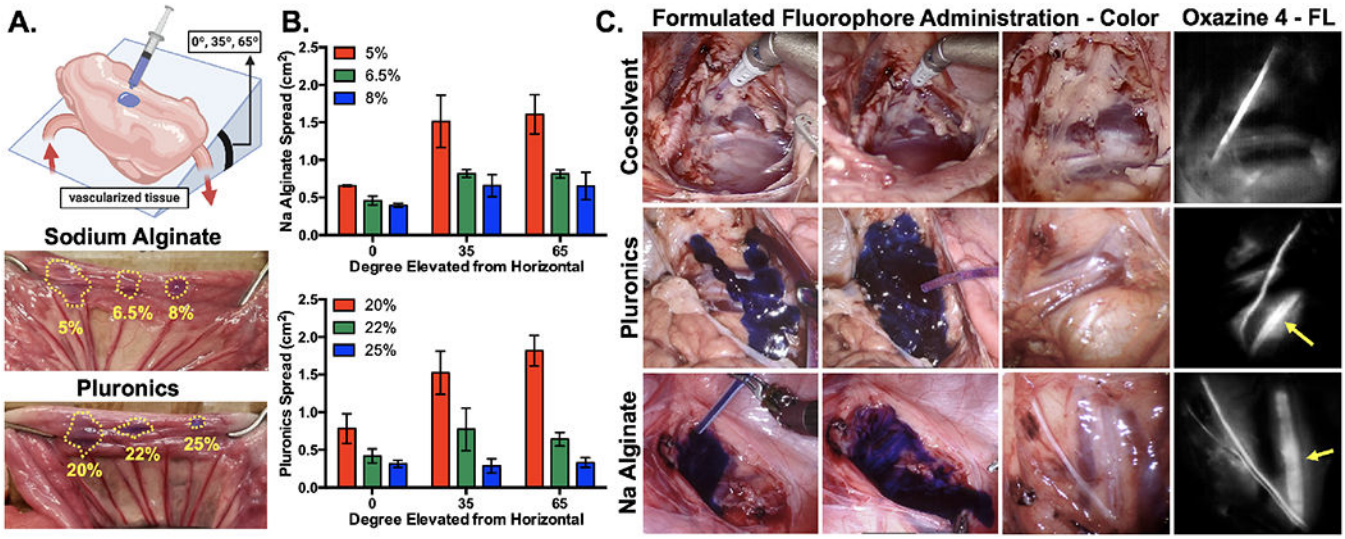

Figure 2: Hydrogel formulation viscosity assessment & large animal model staining studies. **A.** Schematic, representative images, and **B.** quantified tissue spread surface areas for hydrogel formulation viscosity assessment, where Na Alginate (5%, 6.5% and 8%) and Pluronics (20%, 22% and 25%) were evaluated at 0°, 35° and 65° of tilt. The dotted lines indicate the area of tissue spread of each formulation in each representative image. Data is representative of n=3 replicates per formulation and tested tilt angle. **C.** Representative color and fluorescence images of the swine iliac plexus stained via direct administration of co-solvent, 22% Pluronics and 6.5% Na Alginate formulated oxazine 4. Yellow arrows indicate buried nerve tissue visible using fluorescence imaging up to 1 hour after direct administration. FL = fluorescence.

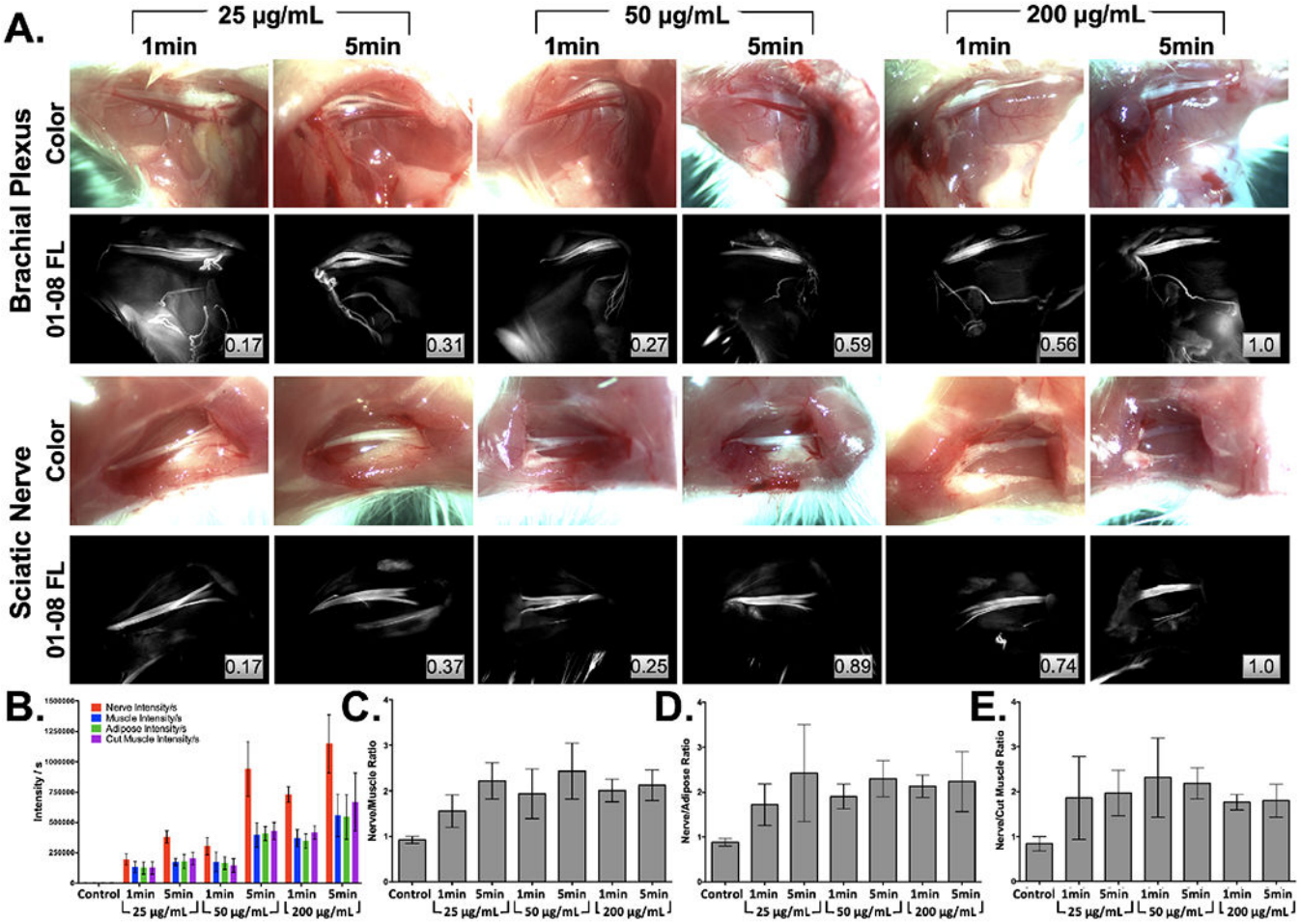

Figure 3: Hydrogel formulation direct administration methodology optimization.

A. Representative brachial plexus and sciatic nerve images following staining with varied concentrations (25, 50 or 200 µg/mL) of LGW01-08 in 22% Pluronics for 1- or 5-mins were **B.** quantified for tissue fluorescence intensity, which was used to calculate **C.** nerve to muscle, **D.** nerve to adipose and **E.** nerve to cut muscle SBR ratios for each tested concentration and incubation time. Images are representative of n=6 nerve sites without normalization. Inset boxes show intensity metrics denoting the fraction of the brightest fluorescence intensity that the image represents between images in the same row. FL = Fluorescence.

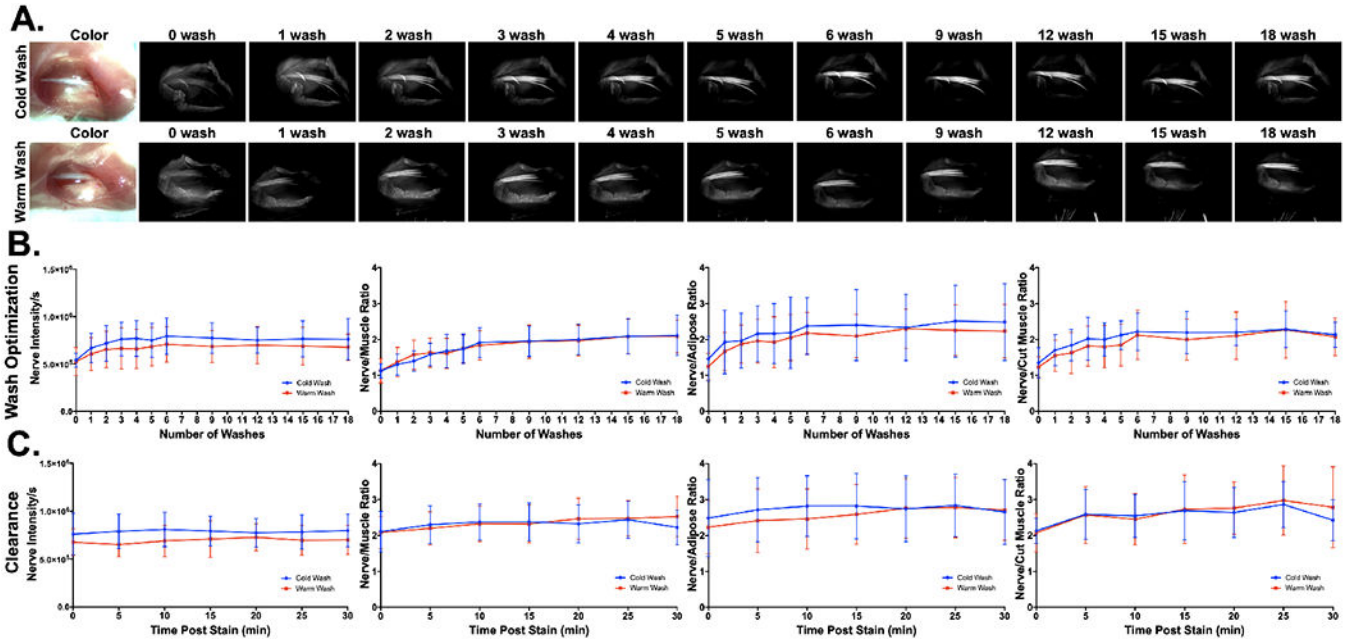

Figure 4: Hydrogel formulation direct administration washing protocol optimization.

A. Representative images and **B.** quantified nerve intensities and SBRs (i.e., nerve to muscle, nerve to adipose and nerve to cut muscle ratios) for wash optimization studies. Room temperature and cold PBS were tested to assess if Pluronics solubility was affected by temperature. All images are representative of data collected for n=6 nerve sites per wash condition, with images collected at 0, 1, 2, 3, 4, 5, 6, 9, 12, 16, and 18 washes. Each wash consisted of a quick flush of the stained tissue region with PBS. **C.** Nerve intensity and SBRs were calculated from images captured for 30 minutes following the final 18th wash step to visualize the effects of clearance on nerve fluorescence intensity and SBRs. All quantified data is presented as mean +/− standard deviation.

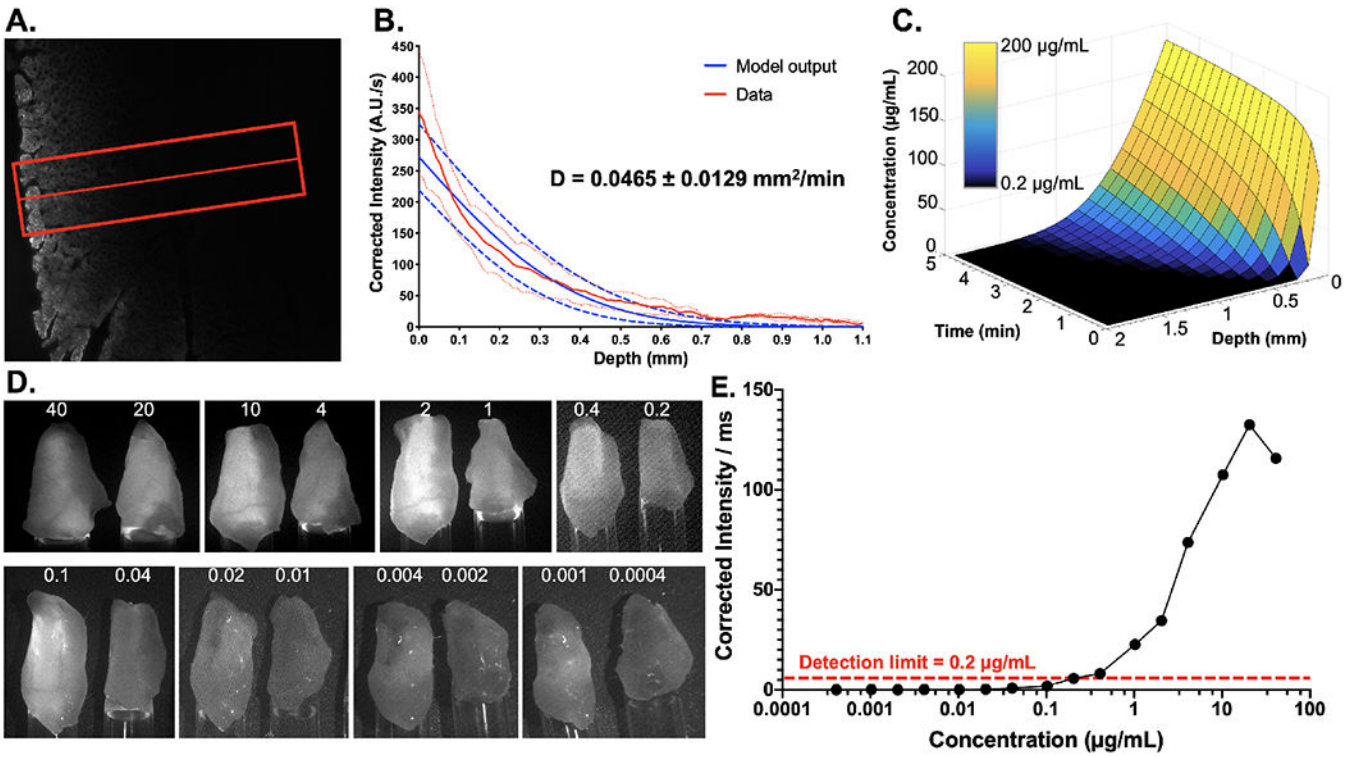

Figure 5: Hydrogel formulation tissue penetration quantification.

A. Representative fluorescence microscopy image of murine muscle tissue cross-section to visualize Pluronics formulated LGW01-08 diffusion after direct administration. The red line and box represent the center line and width used to obtain fluorescence intensity line profiles from the tissue. **B.** Quantified line profiles enabled the calculation of the diffusion coefficient (D) using a mathematical model, which facilitated **C.** prediction of tissue penetration profiles as fluorophore incubation time and concentration were varied. The graph colormap represents the fluorescence visibility at depth, as measured in LGW01-08 reference standards, where black squares represent concentrations at which the fluorescence signal is below the limit of detection at 1 mm of depth. Data is representative of n=9 line profiles and presented as mean +/− standard deviation. **D.** LGW01-08 tissue penetration depth was further estimated using images of LGW01-08 fluorophore in PBS titrated across a range of concentrations (0.0004-40 µg/mL). The varied LGW01-08 concentrations were placed in Eppendorf tubes that were covered with 1 mm of mouse peritoneal muscle tissue and imaged. **E.** Fluorescence intensities were quantified through the overlaying muscle tissue demonstrating that the concentration at which detection of fluorescence over background autofluorescence was 0.2 µg/mL.

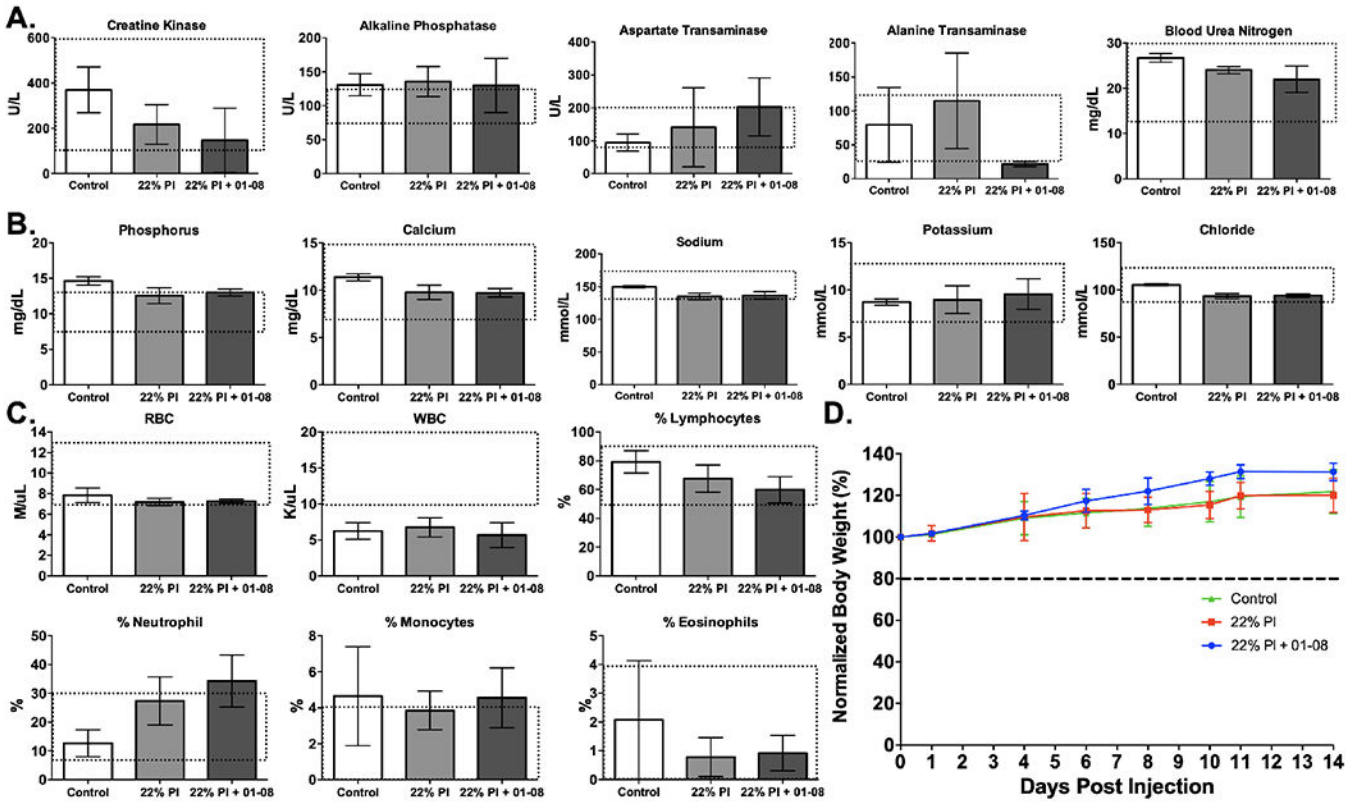

Figure 6: Pluronics formulated LGW01-08 toxicology testing.

A. Blood marker, **B.** electrolyte, and **C.** hematological analysis results represented as concentrations (Units per liter [U/L], milligram per deciliter [mg/dL], millimole per liter [mmol/L], mole per microliter [M/μL], kilo per microliter [K/μL]) or percentages 24 hours following subcutaneous administration of 22% Pluronics either loaded with LGW01-08 for a final dose of 1.8 mg/kg or control unloaded. The dashed line boxes on each graph represent the normal expected range of values. **D.** The measured mean weights for mice up to 14 days after administration of the loaded and unloaded Pluronics gel vs. control un-administered animals. All data are representative of data collected for n=5 mice per group. All quantified data is presented as mean +/− standard deviation.

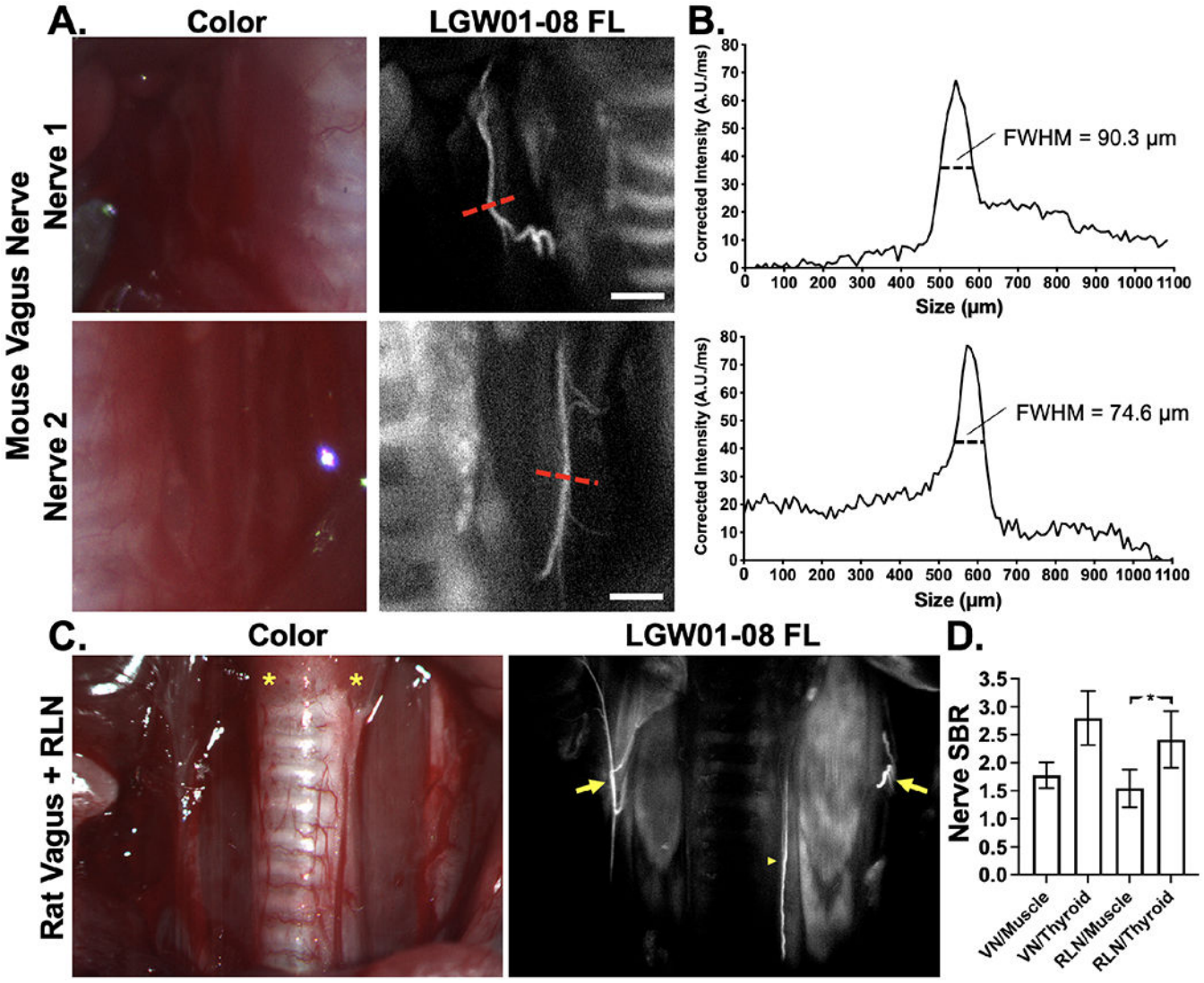

Figure 7: Rodent vagus nerve (VN) and recurrent laryngeal nerve (RLN) staining using the optimized direct administration methodology.

A. Representative images of murine vagus nerve tissue stained following dissection of the trachea with Pluronics formulated LGW01-08 using the optimized direct administration methodology. The displayed images are representative of n=4-stained nerve sites. The red dashed lines indicate where **B.** line profiles were quantified. The full-width-half-maximum (FWHM) were calculated to quantify nerve width, demonstrating visualization of sub-100 µm diameter nerves. **C.** Representative images of rat VN (arrows) and RLN (arrowhead) alongside thyroid (asterisk), trachea, muscle, and vasculature tissue stained following exposure with Pluronics formulated LGW01-08 using the optimized direct administration methodology. The displayed images are representative of n=4 stained nerve sites. **D.** Nerve signal to background ratios (SBRs) were quantified vs. muscle and thyroid tissues. Data is representative of n=4 nerve sites and presented as mean +/− standard deviation. RLN vs.

muscle SBR data was compared to RLN vs. thyroid SBR data to test for significance. * = p value < 0.05. VN = vagus nerve, RLN = recurrent laryngeal nerve.